SPAD-Based Detection System for Nanopore Sequencing Through Surface-Enhanced Raman Spectroscopy

Veronica Storari, Henri Haka, Kirill Khabarov, Simone Tisa, Francesco Tantussi, Francesco De Angelis, Franco Zappa, *Senior Member, IEEE*, and Federica Villa, *Member, IEEE*

***Abstract*—Surface-Enhanced Raman Spectroscopy (SERS) is a powerful technique for molecular identification, based on the correspondence between Raman spectral peaks and the characteristic vibrational modes of the analyte. To intensify the Raman response, SERS relies on nanostructured metallic surfaces, like plasmonic nanopores, that can amplify the electromagnetic field in a highly confined space. When applied to sequencing applications, this approach overcomes the limitations of traditional electrical sensing in biological and solid-state nanopores, offering higher molecular discrimination and enabling fast optical readout. In this work, we propose an experimental setup for protein and DNA sequencing exploiting a Single-Photon Avalanche Diode (SPAD)-based detection system coupled with a custom software application. Our current setup includes plasmonic nanopores, a continuous-wave laser for excitation, gratings to resolve spectral components and a microscope equipped with a SPAD camera for detection. We provide a detailed description of the camera and custom software, followed by preliminary results demonstrating a 10-μs translocation time per nucleotide and highlighting the potential for biomolecules sequencing applications, while outlining the remaining steps needed for single-residue resolution. Future steps include fluorescence background suppression exploiting the SPAD array time-gating feature, and also nanopore and SPAD arrays performance improvement to better control the molecule position and translocation, thus leading to full sequencing capabilities.**

***Index Terms*—DNA, nanopores, plasmonics, proteins, Raman spectroscopy, Surface-Enhanced Raman Spectroscopy (SERS), sequencing, single photon, Single-Photon Avalanche Diode (SPAD), Single-Photon Avalanche Diode (SPAD) arrays.**

I. Introduction

RAMAN Spectroscopy (RS) has played a decisive role in biomedical research for many years. It is a powerful analytical method to detect molecular fingerprints and analyze chemical compositions, which has been used in numerous fields, from pharmaceutical analysis to cancer detection [1], [2]. Its main advantage is the possibility to identify molecules with a label-free approach, as Raman spectra are intimately related to the molecular structure of the sample. Indeed, the Raman effect is a form of inelastic scattering in which a molecule in a given vibrational state undergoes excitation to a virtual state, instantaneously followed by relaxation to a different vibrational state. As illustrated in Fig. 1, this process can result in a scattered photon with lower energy than the incident photon if the initial transition occurs from the ground state to an excited state (Stokes); alternatively, the scattered photon can gain energy if the transition happens in the opposite direction (Anti-Stokes). The energy difference between the incident and the Raman scattered photon is commonly expressed as a wavenumber difference and referred to as the *Raman shift*. This shift corresponds to molecular vibrational modes and appears as characteristic peaks in the Raman spectrum [3].

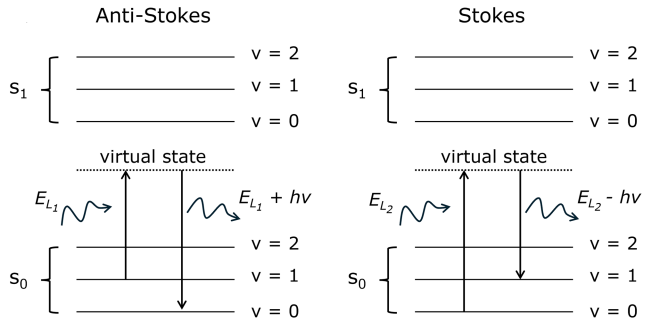

Fig. 1. Raman Scattering diagrams: simultaneous absorption of an incident photon and emission of a scattered Raman photon.

One problem with RS is the low intensity of the signal that carries the information, which makes its use challenging for instance when dealing with single molecules in biological applications. A possible way to increase the Raman signal is the adoption of a slightly modified technique, known as Surface-Enhanced Raman Spectroscopy (SERS), which exploits nanostructured metallic surfaces – typically made of gold or silver – to amplify the electromagnetic signal in their vicinity [4]. To benefit from field enhancement, the molecule needs

Received 21 October 2025; accepted 27 October 2025. Date of publication 3 November 2025; date of current version 19 November 2025. This work was supported in part by the European Union's Horizon 2020 Programme through Project H2020-FETOPEN-2018-2020 under Grant Agreement 964363. *(Corresponding author: Veronica Storari.)*

Veronica Storari, Henri Haka, Franco Zappa, and Federica Villa are with the Dipartimento di Elettronica, Informazione e Bioingegneria, Politecnico di Milano, 20133 Milano, Italy (e-mail: veronica.storari@polimi.it; henri.haka@polimi.it; franco.zappa@polimi.it; federica.villa@polimi.it).

Kirill Khabarov, Francesco Tantussi, and Francesco De Angelis are with the Istituto Italiano di Tecnologia, 16163 Genova, Italy (e-mail: kirill.khabarov@iit.it; francesco.tantussi@iit.it; francesco.deangelis@iit.it).

Simone Tisa is with Micro Photon Devices Srl, 39100 Bolzano, Italy (e-mail: simone.tisa@micro-photon-devices.com).

Digital Object Identifier 10.1109/JPHOT.2025.3628046

to be adsorbed on the substrate or to be very close to it, because the plasmonic resonance that is intensifying the field is highly localized [3]. Therefore, plasmonic nanopores have been proposed as an optimal environment for SERS, providing an amplification of the Raman signal for analytes flowing through highly confined plasmonic gaps [5]. This possibility of coupling SERS with plasmonic nanopores is especially beneficial in the field of biomolecules sequencing, an area where biological and solid-state nanopores have been studied for many years. These structures have been employed to sequence DNA and RNA molecules by monitoring the modulation of the ionic current through the pore at the passage of the different nucleotides [6], [7], [8]. This approach has addressed shortcomings of previous DNA sequencing methods, such as sequencing-by-synthesis, by eliminating the constraints on sequence read length, the need for time-consuming sample preparation and amplification, and the use of fluorescent labels [9], [10].

However, nanopore sequencing based on electrical modulation presents limitations too, in terms of readout speed, identification complexity, and discrimination of other molecular constituents [11], [12], [13].

An optical approach using SERS can overcome these challenges by enhancing the signal and allowing the use of optical detectors. Such detectors are intrinsically faster and capable of keeping up with the biomolecule's translocation times in nanopores, typically in the order of a few microseconds.

In this context, one main aspect must be considered: Raman signal coexists with fluorescence in the same portion of the spectrum, making it impossible to just use optical filters to distinguish between them. Fluorescence emission is intrinsically reduced by the plasmonic effect of the structures adopted for surface enhancement, which have been demonstrated not only to enhance Raman signal, but to actively quench fluorescence if carefully engineered [14], [15], [16]. Another way to mitigate the detrimental effect of fluorescence is the exploitation of the different lifetimes of Raman scattering (picoseconds) and fluorescence emission (hundreds of picoseconds or nanoseconds). This aim can be fulfilled with the adoption of detectors that can be gated, i.e., turned on only when Raman scattering is expected and then turned off right after, to temporally mask the majority of fluorescence signal [17], [18], [19]. When gated detectors are employed to reduce fluorescence contributions to the spectrum, the continuous wave lasers used in traditional RS setups must be replaced with sub-nanosecond pulsed lasers to properly synchronize the analyte excitation with the gate signal window [20], [16].

To reconstruct a spectrum, different wavelengths must be distinguished. This is usually achieved using an excitation laser with a narrow spectral linewidth and a diffraction grating that can spatially separate the wavelengths of the scattered light (Fig. 2). A detection system based on a detector array is then needed to capture the different wavelengths simultaneously, ensuring a sufficiently high readout speed. These arrays typically have a linear geometry, which allows them to capture the resolved spectral components, but sometimes they include a few pixels in a second dimension to account for the width of the laser beam. Various detectors have been employed in RS measurements,

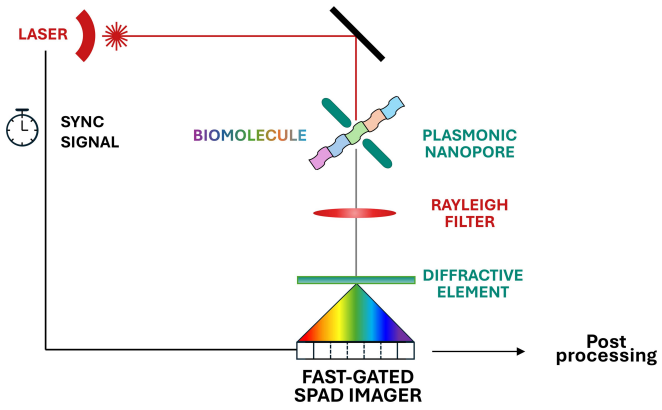

Fig. 2. Proposed detection system for protein and DNA sequencing using SERS in nanopores. The synchronization signal is required only in pulsed laser setups, when exploiting the SPAD time-gating feature.

starting from Photomultiplier Tubes (PMTs) and Multichannel Plate PMTs (MCP-PMTs). PMTs are unsuitable for the fast spectral acquisitions required by sequencing applications because they are single-point detectors. MCP-PMTs overcome the limitations in spectral resolution, but they require high bias voltages and suffer from rapid aging [17], [19], [21]. More recently, other detectors have been used for RS, such as Intensified and Electron-Multiplying Charge-Coupled Devices (ICCDs and EMCCDs). ICCDs offer fast electronic gating, but they feature low readout speed, and, since they include an MCP, they require high bias voltages and are prone to aging. EMCCDs cannot be directly gated, but they have higher efficiencies. Unfortunately, they also suffer from high dark current noise and need cooling to operate [18], [19], [22]. High-frame-rates alternatives for RS are Scientific Complementary Metal Oxide Semiconductors (sCMOS) cameras and silicon Single-Photon Avalanche Diode (SPAD) arrays. Both can operate at low voltages and without cooling, which makes them less power-consuming and less expensive than the previously presented options. The limited efficiency of SPADs has been mitigated with microlenses and advancements in manufacturing technology. The inherently digital output of SPAD arrays eliminates the readout noise, making them well-suited for single-photon detection at short integration times, which is the case of RS for biomolecule sequencing [17], [23], [24], [25]. Another important aspect for RS is that SPAD arrays often implement integrated nanosecond gating [23]. Although this gate width might be larger than desired for RS of samples with a low Raman-to-fluorescence ratio, double-gating techniques have been proposed to address the finite time needed to switch SPAD detectors on and off. A *hard gate* with nanosecond width can be applied directly to SPADs, switching them on and off, while a second *soft gate* applied just to the readout can effectively achieve sub-ns windows [20], [26].

Advancements in the fabrication of plasmonic nanopores and the continuously improving resolution offered by high-efficiency detector arrays bring the practical application of SERS to perform DNA and protein sequencing closer than ever. To contribute to the research in this field, we present an experimentally validated detection system based on a SPAD array,

designed to perform DNA and protein sequencing exploiting SERS in plasmonic nanopores. DNA and proteins are passed through plasmonic nanopores where they are excited with a laser beam, nucleotide by nucleotide or amino acid by amino acid. The resulting secondary radiation is directed towards a diffractive element to spatially separate the spectral components, to be collected through a suitable SPAD camera.

The paper is organized as follows: Section II describes the adopted SPAD camera with a focus on the microlens array performance. Section III presents the software developed for the project. Section IV introduces the experimental setup together with some preliminary results. Further details on the experimental discussion are available in recently published works. The presented nanopore is characterized in depth in [27], while additional biological results obtained with the described detection system are reported both in [27] and [28].

II. SPAD Camera

The SPAD camera employed in this work is a commercial module by Micro Photon Devices (MPD) [29], selected to effectively meet the requirements of sequencing applications using SERS, in terms of speed, sensitivity and time-gating availability. It operates in global shutter mode and can reach a maximum frame rate of about 10^5 frames per second with a 9-bit depth and at full resolution (i.e., 64 $\times$ 32 pixels). This frame rate results in a minimum acquisition time of 10.4 μs, which corresponds to the typical translocation time of one or two single units – amino acid or DNA base – in the experimental configuration adopted for this article. Longer integration times can be obtained by accumulating 10.4 μs frames at hardware level.

This camera supports both free-running and gated operating modes, enabling different fluorescence filtering techniques. Therefore, it can be used in both continuous-wave and pulsed laser setups. When operated in gated mode, the gate signal presents rise/fall times of 500 ps and a repetition period of 20 ns. It can be either provided externally with a minimum window of 5 ns or it can be generated internally with a minimum active window of 1.5 ns. In this second case, the signal delay can be adjusted with a resolution of 20 ps. The gate width allowed by this camera, especially the internally generated one, are well-suited for fluorescence rejection in Raman applications. Even if the optimal width of the gating signal depends on the fluorescence lifetime of the sample, this effect is more critical for samples with low Raman-to-fluorescence ratio [20]. In our SERS setup, plasmonic nanopores already reduce the fluorescence signal and enhance the Raman one, relaxing the contraints on the optimal width of the gate window. The camera also exhibits gating skews of 200 ps between the central pixels and those at the edges, that could affect the acquired spectra quality. This effect could become limiting for samples with low Raman-to-fluorescence ratio [30]. However, the distortion introduced by gating skews becomes less critical as the Raman-to-fluorescence ratio increases, like in the case of SERS.

The camera is based on an Application-Specific Integrated Circuit (ASIC) with a 64 $\times$ 32 pixel array, previously designed by Politecnico di Milano [31]. Being two-dimensional, the form factor of the chosen camera is not typical for RS applications. However, the values of only a few rows out of the 32 available ones are considered during processing, while the 64 columns can provide a satisfactory spectral resolution of 10 cm^{-1} over approximately 650 cm^{-1} of bandwidth, using a standard spectrometer grating of 1800 grooves/mm and a laser wavelength of 532 nm.

For this ASIC, every pixel comprises a SPAD sensor, a front-end circuit to properly bias the SPAD and some digital logic circuitry. The front-end circuit is based on a Variable-Load Quenching Circuit (VLQC) topology optimized for noise reduction and is described in detail in [31], while the digital logic includes three counters, connected to the readout circuit. This integrated circuit was designed in a 0.35-μm, planar CMOS technology, so the presence of electronics inside the pixel is limiting the Fill-Factor (FF), i.e., the ratio between the SPAD active area and the pixel area. With a pixel pitch of 150 μm and a SPAD diameter of 30 μm, the resulting FF is 3.14%. The overall electronic system is enclosed in a case and it was integrated into the optical setup with a Thorlabs SM1 thread, a C-mount mechanical adapter and a high-speed USB 3.0 computer interface.

Especially in photon-starved applications like RS of biological samples, the detector efficiency is a key parameter to evaluate. Two figures of merit can be investigated with this aim: the Photon Detection Probability (PDP) and the Photon Detection Efficiency (PDE). The first one is defined as the ratio between the generated avalanche pulses and the photons that are reaching the SPAD active area, while the second one accounts also for the efficiency reduction due to the native FF and for possible improvements given by the introduction of microlenses [21], [33].

The low FF of this array would drastically impact its PDE, but it has been improved with the introduction of a Micro-Lens Array (MLA) to focus incoming photons from all over the pixel area onto the SPAD active area [33].

The performance of the MLA can be evaluated through the Concentration Factor (CF), which expresses the increase in collected light power when the MLA is imprinted onto the detector [34]. For this camera, the MLA exhibited non-uniformities of less than 5%, without any evident spatial pattern. This low level of non-uniformity allows the computation of a single effective FF for the entire array, which can be calculated by multiplying the native FF by the CF.

This effective FF is higher than the native one and depends on the aperture of the incoming beam, as shown in the simulations of Fig. 3. When a collimated beam is used, the FF recovers up to 75.4%. The effective FF was simulated at three different wavelengths (400 nm, 600 nm and 800 nm), and, since no significant variations were observed, an average of the three different curves is displayed in the plot in Fig. 3. For this camera, the native PDE – experimentally measured for a camera sample without the MLA – is shown in Fig. 4, while 5 shows the measured PDE for the camera with the MLA, evaluated at three different apertures of the incoming beam (3.05°, 7.63°, 18.92°). The PDE of the camera after the introduction of the MLA greatly improves, especially when collimated beams are used, experimentally proving the expected performance of the MLA. Indeed, the experimental ratio between the final and native

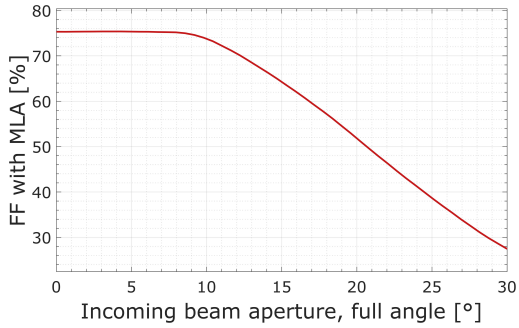

Fig. 3. Simulated FF of the 64 × 32 SPAD camera as a function of the incoming beam aperture after the introduction of the MLA.

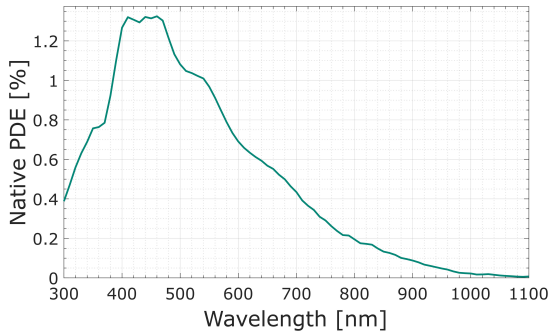

Fig. 4. Native PDE of the 64 × 32 SPAD camera. Measurements taken at 35°C, with the SPADs biased 5 V above the breakdown voltage.

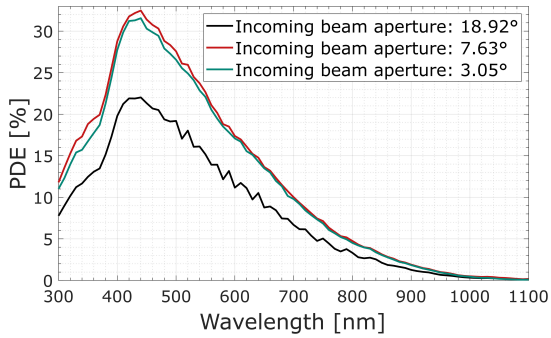

Fig. 5. PDE of the 64 × 32 SPAD camera with MLA, as a function of the incoming beam aperture (full angle). Measurements taken at 35°C, with the SPADs biased 5 V above the breakdown voltage.

PDEs corresponds to the ratio between the simulated effective FF and the native one.

The camera achieves state-of-the-art performance in terms of Dark Count Rate (DCR). This figure of merit expresses the average avalanche rate when the sensor is kept in dark conditions, i.e., when the avalanches are caused by thermal generation and tunneling events [32]. With a SPAD active-area diameter of 30 μm and a 5 V excess bias voltage, the device yields a mean DCR of 425 cps, with 97% of pixels that count less than 1 kcps in dark conditions [31]. Such a low DCR also positively impacts the Dynamic Range (DR). DR is defined as the ratio between the maximum signal that can be sensed by the detector and the minimum signal that it can detect. A mean DCR of 425 cps keeps the minimum detectable signal at 1 count, even for integration times as long as 2.3 ms. As a result, the SPAD array achieves a DR of 54 dB, that can be extended for the camera up to 94 dB by summing multiple frames at the system level, increasing the maximum photon count [31].

III. Software and Processing

The experimental measurements carried out in this project require careful alignment between the plasmonic nanopore and the optical system with the camera. The substrate active area was designed to match the Point Spread Function (PSF) of the optical system, approximately 500 nm × 1500 nm, to maximize the number of detected events. Any misalignment would result in signal loss, thus making real-time visualization of the acquired spectra and their time-evolution essential for an effective alignment. Therefore, we developed a software solution specifically targeted at RS, which includes a live visualization of the data being acquired. The software application – developed in C++ – includes firmware to communicate with the camera, a pre-processing pipeline of the data stream and a Graphical User Interface (GUI) for real-time plotting.

The firmware is based on a set of functions included in MPD's Dynamic Linked Library (DLL) through which the camera is activated in the desired working modality and the integration time is set. While an acquisition is running, the data are continuously downloaded from the camera and saved in a memory buffer, waiting for pre-processing. The firmware is also responsible for starting and stopping the acquisitions on user request.

The pre-processing consists in two phases: the hot pixel compensation and the data compression. The position of hot pixels is known for a specific camera thanks to an initial calibration process where the Dark Count Rate (DCR) of every pixel is recorded by performing a measurement in complete darkness with the camera shutter closed. Those pixels showing a DCR higher than two times the average DCR are considered hot pixels. During a normal acquisition, the hot pixel compensation is then performed by substituting the outlier value with an average of the values of the two closest non-hot pixels. By using an average value, we avoid any distortion in the color-coded plot, for which the hue scale self-adjusts. The data compression allows to display and save only useful data. In this phase, every 64 × 32 pixel frame is reduced to a single 64 pixel frame by summing across a user-defined subset of rows. Indeed, as mentioned in Sections I and II, spectroscopy applications usually require linear acquisition systems, therefore not all the 32 rows of the camera carry relevant information, but just a small subset of them is needed – typically from 2 to 4 rows – to account for the width of the light beam collected by the optical system. Hence, by summing the value of different pixels within each column, we create a 64 pixel array where every element carries all the information related to a specific Raman shift. The use of a limited number of rows is also beneficial, as it allows selecting regions of the array with a hot-pixel number below the statistical average, reducing the risk of defective spectra. The resulting data are then saved locally in a text file, to have them for further post-processing elaboration.

The GUI (shown in Fig. 6) is based on the open source "ImGui" library and creates a user-friendly environment to

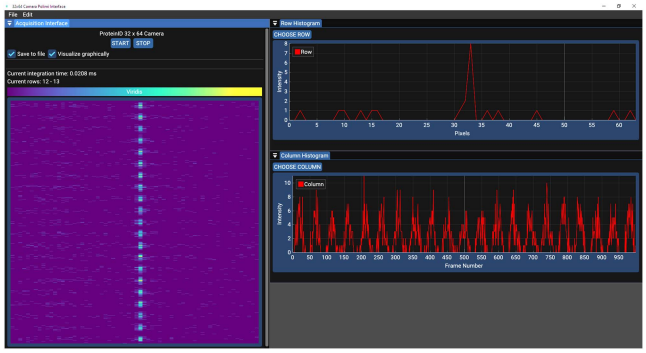

Fig. 6. GUI showing real-time acquisition with 20.8 μs integration time. A crystalline silicon sample (Raman peak at 520 cm^{-1}) is excited with a laser modulated by a chopper at 1000 Hz to generate a predictable signal. (Left) Color-coded plot where every line corresponds to a 64-pixel frame and the most recent data are shown on top. (Right) 2-D plots of intensities along a row (top) and along a column (bottom).

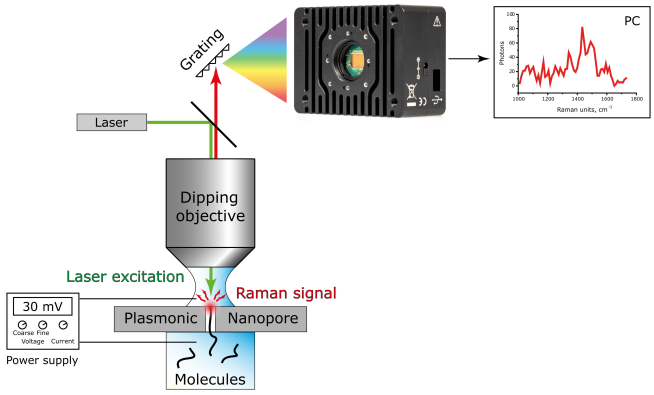

Fig. 7. Experimental Setup. A potential difference drives biomolecules through the nanopore, where they are excited by a continuous-wave laser. The light scattered by the analyte is recorded by a 64 × 32 SPAD camera, operated via custom software for real-time monitoring.

communicate with the camera. It includes the possibility to set the integration time of the single acquisition, to start and stop a measurement and to select the subset of rows to work on. The interface also includes three different plots for data visualization. The main plot is a color-coded representation of the acquired intensity that updates every time a new frame is available, putting new data on top, like in a waterfall. It shows 1000 frames at a time, corresponding to the simultaneous visualization of about 20 ms of acquisitions, with an integration time of 20.8 μs. On the side of this plot, there are two real-time 2D-representations of intensity: the first displays intensity along a row (i.e., spectrum of the incoming light as a function of the Raman shift) and the second along a column (i.e., time evolution of light intensity detected by each column).

To maximize the download and processing speed, the software is based on a multi-thread approach. Specifically, three threads are present in the software: the first thread takes care of downloading, preprocessing and saving the data, the second thread handles the shifting operation for the color-coded plot update while the third one is dedicated to rendering only. Although the maximum frame rate of the camera could not be reached with the overhead introduced by preprocessing and visualization, acquisition times down to 20.8 μs could be effectively processed and rendered in real time, allowing for prompt monitoring of the experiment.

Once the data are saved, they are post-processed with a custom Python script to reduce noise, detect translocation events and subtract background and fluorescence. Noise reduction is implemented through a 2D (space and time) Wiener filtering algorithm. Frames with translocation events are selected with a threshold based on the 99th percentile of total photon count per measurement. Finally, background and fluorescence are reduced by subtracting the average baseline.

IV. Experimental Measurements

A customized setup was devised to carry out experimental measurements. For the results presented in this work, we adopted a cost-effective continuous wave laser, therefore relying only on a plasmonic quenching of fluorescence.

The 64 × 32 SPAD camera is mounted on a commercial Raman microscope (InVia, Renishaw) providing continuous spectral acquisitions, motorized control at the sample stage and objective movements. The excitation and collection are performed directly with a water dipping 63× objective (Leica HC APO L 63x/090 W U-V-I) to increase the collection efficiency and minimize background signal. Three different laser wavelengths are available in the setup – 532 nm, 633 nm and 785 nm – to allow the selection of the one exciting the strongest Raman signal depending on the plasmonic properties of the nanopore. The plasmonic membrane with nanopores is positioned between two chambers – one, close to the objective, filled with a NaCl 150 mM buffer solution only, and the other on the opposite side of the membrane with the studied analyte dissolved in the same buffer. To ensure that molecules pass through the nanopores via electrophoresis, a constant voltage of 100 mV is applied between two Ag/AgCl electrodes immersed in the solutions on the opposite sides of the plasmonic film, generating an electric field. The actual measurements are performed under the laser irradiation focused on the nanopore with an optical power of about 1 mW (corresponding to an optical power density of 40 kW/cm^2). The schematic of an experimental setup is shown in Fig. 7.

To demonstrate the performance of the system we used a 1 nM solution of poly-cytosine molecule (polyC), consisting of 30 repeating cytosines connected through the DNA backbone, an alternating chain of deoxyribose and phosphate groups. Collecting hundreds of translocation spectra within a range of 950-1600 cm^{-1} we calculated the average SERS spectrum of polyC (Fig. 8(a)) and statistically estimated the translocation efficiency. It should be noted that SERS can shift and enhance different vibrational modes, not only relative to normal RS, but also among different SERS approaches, because of the specific surface geometry and chemical enhancement. Therefore, the acquired spectrum may differ from those reported in other studies. The photon count distribution for the investigated molecule is presented in Fig. 8(b). Under the adopted experimental conditions, we observed the most probable Raman scattering rate of 270 photons per molecule, which corresponds to 9 photons detected per single nucleotide. Considering the overall efficiency of the setup estimated around 5–10% by including lenses and

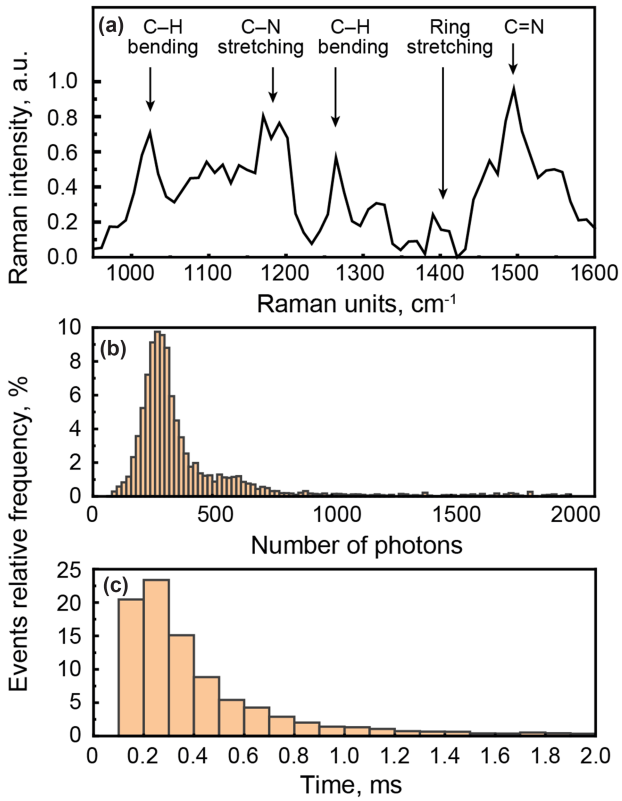

Fig. 8. Averaged SERS spectra (a) and translocation statistics for polyC molecule at 1 nM concentration acquired with 100 μs time resolution: distributions of photons emitted during the detected translocations (b) and translocation time distribution (c).

camera efficiencies in the spectral range of interest for the 532 nm excitation, the actual number of emitted Raman photons is considerably higher than the number we collected with the current setup. The distribution of translocation times, reported in Fig. 8(c), shows a median value of 300 μs for polyC molecules consisting of 30 nucleotides. This result corresponds to roughly 10 μs translocation time per single nucleotide.

Even though the presented SPAD camera allows integration times down to 10 μs, the overall efficiency of the system is insufficient to achieve a satisfactory Signal-to-Noise Ratio (SNR) in such a short time. Therefore, a 100 μs integration time was selected to characterize the nanopore behavior and highlight the potential of the proposed experimental setup for molecule identification. To make this system viable for sequencing applications, further improvements are required to increase the SNR of the performed measurements. The camera's DCR is already negligible with respect to the detected signal: measuring 9 photons per 10-μs translocation, we have a signal rate of 900 kcps – more than three order of magnitude above the DCR. SNR improvements can be pursued by using a pulsed laser to exploit the time-gating capability of the camera with the aim of reducing the fluorescence background. In fact, subtraction of the average fluorescence is already performed at the post-processing stage; what could further improve the spectral quality is the removal of fluorescence variance, which cannot be accomplished after acquisition. In addition, ongoing advances in nanopore fabrication – like the integration of multiparticle assemblies in the pores [28] – could be exploited to make the Raman signal enhancement more effective. Additional experimental measurements focusing on the sequencing capabilities of the described setup are available in recently published papers [27], [28].

V. Conclusion

In this paper, we presented a detection system based on a SPAD camera designed to perform high-speed protein and DNA sequencing in nanopores exploiting SERS. We also developed a customized software application for data acquisition, and we provided a detailed description of the experimental setup and the obtained results.

The employed SPAD camera has a maximum frame rate of 100 kfps, making it suitable to perform fast sequencing in nanopores through SERS. Indeed, the camera frame rate corresponds to a minimum integration time of 10 μs, that, combined with the 10 μs per nucleotide translocation time of our plasmonic nanopores, can allow for the recording of spectra from one or two residues at a time. Although single residue resolution has not yet been achieved, this result is comparable to the state-of-the-art sequencing instrumentation based on electrical readout, which can reach a two-residue step in protein translocation. Remarkably, state-of-the-art electrical readouts are considerably slower, with single amino acid dwell times in nanopores in the order of tens of milliseconds while our approach has proven to reach dwell times in the order of few microseconds [35], [36]. This speed advantage, combined with the superior discrimination power of SERS, suggests strong potential for our solution in biomolecule sequencing.

The prospective improvements in fluorescence rejection due to the addition of time gating on top of plasmonic enhancement were not addressed in this study and will be considered in future investigations. The gate width offered by this camera agrees well with SERS requirements, as gating times in the order of nanoseconds have been proven to greatly reduce fluorescence contribution to the spectra when applied as a standalone fluorescence rejection method [20]. Although the camera exhibits some limitations in gate skews among pixels and in rise and fall times of the gate, as explained in Section II, plasmonic effects already provides substantial fluorescence rejection, making these requirements less critical in nanopore sequencing. Therefore, we plan to further investigate the possibility of combining multiple fluorescence-rejection methodologies to increase the quality of the acquired Raman spectra.

Some improvements can still be made to our system, starting with the plasmonic nanopore, as well as the external environment where the translocation occurs and the electrophoretic driving, which could be optimized to better control the motion of translocating molecules. This is particularly relevant for shorter molecules, which do not always translocate with the correct orientation and, as a result, cannot fully benefit from plasmonic hot spot enhancement.

In the future, a dedicated detector could be designed specifically for SERS-based sequencing applications. It could feature a linear SPAD array, avoiding the excess of data caused by the

use of a bidimensional camera, thereby increasing the data rate and enabling faster acquisitions with real-time monitoring. The adoption of more advanced technological nodes would enable faster gating and higher PDE. In particular, 3D-stacked technologies – with an imaging-dedicated top tier and a bottom tier reserved for the electronics – would be beneficial in maximizing the FF.

Overall, this work shows the potential of a plasmonic nanopore environment for sequencing applications, proving that SPAD sensors have the optimal time resolution for such applications and highlighting the validity of the proposed setup as an alternative to electrical readout. Our future research will address the limitations of the current setup, aiming to achieve optimal system performance to enable sequencing with single-residue resolution.

REFERENCES

[1] T. Vankeirsbilck et al., "Applications of Raman spectroscopy in pharmaceutical analysis," *TrAC Trends Anal. Chem.*, vol. 21, no. 12, pp. 869–877, Dec. 2002, doi: 10.1016/S0165-9936(02)01208-6.

[2] G. W. Auner et al., "Applications of Raman spectroscopy in cancer diagnosis," *Cancer Metastasis Rev.*, vol. 37, pp. 691–717, Dec. 2018, doi: 10.1007/s10555-018-9770-9.

[3] E. Le Ru and P. Etchegoin, *Principles of Surface-Enhanced Raman Spectroscopy and Related Plasmonic Effects*, 1st ed. Amsterdam, The Netherlands: Elsevier, 2009, doi: 10.1016/B978-0-444-52779-0.X0001-3.

[4] L. Guerrini and D. Graham, "Molecularly-mediated assemblies of plasmonic nanoparticles for surface-enhanced Raman spectroscopy applications," *Chem. Soc. Rev.*, vol. 41, no. 21, pp. 785–717, Oct. 2012, doi: 10.1039/c2cs35118h.

[5] H. L. Liu, K. Zhan, K. Wang, and X. H. Xia, "Recent advances in nanotechnologies combining surface-enhanced Raman scattering and nanopore," *TrAC Trends Anal. Chem.*, vol. 159, Feb. 2023, Art. no. 116939, doi: 10.1016/J.TRAC.2023.116939.

[6] M. Wanunu, "Nanopores: A journey towards DNA sequencing," *Phys. Life Rev.*, vol. 9, no. 2, pp. 125–158, Jun. 2012, doi: 10.1016/J.PLREV.2012.05.010.

[7] D. Branton et al., "The potential and challenges of nanopore sequencing," *Nature Biotechnol.*, vol. 26, no. 10, pp. 1146–1153, Oct. 2009, doi: 10.1038/nbt.1495.

[8] E. A. Manrao et al., "Reading DNA at single-nucleotide resolution with a mutant MspA nanopore and phi29 DNA polymerase," *Nature Biotechnol.*, vol. 30, no. 4, pp. 349–353, Apr. 2012, doi: 10.1038/nbt.2171.

[9] J. Shendure et al., "DNA sequencing at 40: Past, present and future," *Nature*, vol. 550, pp. 345–353, Oct. 2017, doi: 10.1038/nature24286.

[10] T. Hu, N. Chitnis, D. Monos, and A. Dinh, "Next-generation sequencing technologies: An overview," *Hum. Immunol.*, vol. 82, no. 11, pp. 801–811, Nov. 2021, doi: 10.1016/j.humimm.2021.02.012.

[11] M. Iarossi et al., "High-density plasmonic nanopores for DNA sensing at ultra-low concentrations by plasmon-enhanced Raman spectroscopy," *Adv. Funct. Mater.*, vol. 33, no. 41, Oct. 2023, Art. no. 2301934, doi: 10.1002/adfm.202301934.

[12] M. Belkin, S. H. Chao, M. P. Jonsson, C. Dekker, and A. Aksimentiev, "Plasmonic nanopores for trapping, controlling displacement, and sequencing of DNA," *ACS Nano*, vol. 9, no. 11, pp. 10598–10611, Nov. 2015, doi: 10.1021/acsnano.5b04173.

[13] K. A. Kang, J. Wang, J. B. Jasinski, and S. Achilefu, "Fluorescence manipulation by gold nanoparticles: From complete quenching to extensive enhancement," *J Nanobiotechnology*, vol. 9, May 2011, Art. no. 16, doi: 10.1186/1477-3155-9-16.

[14] D. Ghosh and N. Chattopadhyay, "Gold and silver nanoparticles based superquenching of fluorescence: A review," *J. Lumin.*, vol. 160, pp. 223–232, Apr. 2015, doi: 10.1016/j.jlumin.2014.12.018.

[15] Y. Chen, K. Munechika, and D. S. Ginger, "Dependence of fluorescence intensity on the spectral overlap between fluorophores and plasmon resonant single silver nanoparticles," *Nano Lett.*, vol. 7, no. 3, pp. 690–696, Mar. 2007, doi: 10.1021/nl062795z.

[16] D. Wei, S. Chen, and Q. Liu, "Review of fluorescence suppression techniques in Raman spectroscopy," *Appl. Spectrosc. Rev.*, vol. 50, no. 5, pp. 387–406, 2015, doi: 10.1080/05704928.2014.999936.

[17] M. Kögler and B. Heilala, "Time-gated Raman spectroscopy – A review," *Meas. Sci. Technol.*, vol. 32, no. 1, 2021, Art. no. 012002, doi: 10.1088/1361-6501/abb044.

[18] A. Chiuri and F. Angelini, "Fast gating for Raman spectroscopy," *Sensors*, vol. 21, no. 8, 2021, Art. no. 2579, doi: 10.3390/s21082579.

[19] F. Madonini and F. Villa, "Single photon avalanche diode arrays for time-resolved Raman Spectroscopy," *Sensors*, vol. 21, no. 13, Jul. 2021, Art. no. 4287, doi: 10.3390/s21134287.

[20] I. Nissinen, J. Nissinen, P. Keränen, and J. Kostamovaara, "On the effects of the time gate position and width on the signal-to-noise ratio for detection of Raman spectrum in a time-gated CMOS single-photon avalanche diode based sensor," *Sensors Actuators B: Chem.*, vol. 241, pp. 1145–1152, 2017, doi: 10.1016/j.snb.2016.10.021.

[21] A. S. Tremsin, J. V. Vallerga, and O. H. W. Siegmund, "Overview of spatial and timing resolution of event counting detectors with microchannel plates," *Nucl. Instrum. Methods Phys. Res. Sect. A: Accelerators, Spectrometers, Detectors Assoc. Equip.*, vol. 949, Jan. 2020, Art. no. 162768, doi: 10.1016/J.NIMA.2019.162768.

[22] W. Zhang and Q. Chen, "Signal-to-noise ratio performance comparison of electron multiplying CCD and intensified CCD detectors," in *Proc. Int. Conf. Image Anal. Signal Process.*, 2009, pp. 337–341, doi: 10.1109/IASP.2009.5054588.

[23] C. Bruschini, H. Homulle, I. M. Antolovic, S. Burri, and E. Charbon, "Single-photon avalanche diode imagers in biophotonics: Review and outlook," *Light Sci. Appl.*, vol. 8, p. 87, Dec. 2019, doi: 10.1038/s41377-019-0191-5.

[24] W. J. N. Klement, P. Leproux, W. R. Browne, and H. Kano, "CMOS and CCD detection in Raman spectroscopy: A comparison using spontaneous and multiplex coherent anti-stokes Raman scattering (CARS)," *J. Raman Spectrosc.*, vol. 56, no. 9, pp. 933–938, 2025, doi: 10.1002/jrs.6773.

[25] V. Krishnaswami, C. J. F. Van Noorden, E. M. M. Manders, and R. A. Hoebe, "Towards digital photon counting cameras for single-molecule optical nanoscopy," *Opt. Nanoscopy*, vol. 3, 2014, Art. no. 1, doi: 10.1186/2192-2853-3-1.

[26] V. Storari, A. A. Maurina, H. Haka, F. Madonini, I. Cusini, and F. Villa, "40-nm SPAD-array detection system for ultra-fast Raman spectroscopy," in *Proc. Microsc. Histopathol. Analytics*, 2024, pp. JS4A–JS11, doi: 10.1364/TRANSLATIONAL.2024.JS4A.11.

[27] K. Khabarov et al., "Raman identification of single nucleotides flowing through permeable plasmonic films," *Nature Commun.*, no. 16, Oct. 2025, Art. no. 9113, doi: 10.1038/s41467-025-64165-9.

[28] F. K. Sarbishe et al., "High-speed Raman readout of single polypeptides via plasmonic nanopores," *Adv. Mater.*, vol. 37, 2025, Art. no. 2504436, doi: 10.1002/adma.202504436.

[29] Micro Photon Devices s.r.l., "Hermes." Accessed: Oct. 2025. [Online]. Available: https://www.micro-photon-devices.com/products/arrays/hermes

[30] J. Kekkonen, T. Talala, J. Nissinen, and I. Nissinen, "On the spectral quality of time-resolved CMOS SPAD-based Raman spectroscopy with high fluorescence backgrounds," *IEEE Sensors J.*, vol. 20, no. 9, pp. 4635–4645, May 2020, doi: 10.1109/JSEN.2020.2966119.

[31] D. Bronzi et al., "100 000 frames/s 64 × 32 single-photon detector array for 2-D imaging and 3-D ranging," *IEEE J. Sel. Topics Quantum Electron.*, vol. 20, no. 6, Nov./Dec. 2014, Art. no. 3804310, doi: 10.1109/JSTQE.2014.2341562.

[32] I. Cusini et al., "Historical perspectives, state of art and research trends of single photon avalanche diodes and their applications (Part 1: Single pixels)," *Front. Phys.*, vol. 10, Jun. 2022, Art. no. 906675, doi: 10.3389/fphy.2022.906675.

[33] I. Cusini et al., "Historical perspectives, state of art and research trends of SPAD arrays and their applications (Part II: SPAD arrays)," *Front. Phys.*, vol. 10, Jul. 2022, Art. no. 906671, doi: 10.3389/fphy.2022.906671.

[34] S. Donati, G. Martini, and M. Norgia, "Microconcentrators to recover fill-factor in image photodetectors with pixel on-board processing circuits," *Opt. Exp.*, vol. 15, no. 26, pp. 18066–18075, Dec. 2007, doi: 10.1364/OE.15.018066.

[35] K. Motone et al., "Multi-pass, single-molecule nanopore reading of long protein strands," *Nature*, vol. 633, pp. 662–669, Sep. 2024, doi: 10.1038/s41586-024-07935-7.

[36] Y. Zhao, M. Iarossi, A. F. De Fazio, J. A. Huang, and F. De Angelis, "Label-free optical analysis of biomolecules in solid-state nanopores: Toward single-molecule protein sequencing," *ACS Photon.*, vol. 9, no. 3, pp. 730–742, Mar. 2022, doi: 10.1021/acsphotonics.1c01825.